Breathe In: Mucolytic treatment and Drug Discovery Pipeline against antibiotic resistant bacterial strains in Cystic Fibrosis

Juaréz J.A[1], Hernández A[1], Diosdado A[1], Díaz D[1], Leyva S[1], Espinoza D[1], Escobar M[1], Cuellar D[1], Betancourt V[1], Lomelí I[1], Velázquez F[1], Wells G[1], Anaya A[1], Vera R[1], Macías A[1], Estrada D[1], Juaréz L[2], Guzmán E[2], Zesati R[2], García R[2], Cassani C[3], Cabrera H[3] and Alcaráz C[3]

[1]Department of Biotechnology , Tecnologico de Monterrey

October 30, 2019

Abstract

Cystic fibrosis(CF) is a progressive genetic disease that, through the production of abnormally thick mucus, causes degeneration of lung conditions and induces the proliferation of multidrug resistant bacterial strains (MRBS). The combination of treatments with antibiotics and mucolytics has become an alternative for treatements against P. aeuroginosa, an opportunist pathogen that grows in the respiratory tract of CF patients and has become their principal cause of death.

We present a conceptual pipeline for the discovery of antibiotics using a variety of whole-cell biosensors that, when co-cultivated with secondary metabolite producers, sense the presence of antibiotics and the possible chemical identification of such compounds, using a microfluidic system coupled to a mass-spectrometer; as well as a new treatment using a neuraminidase as a mucolytic to reduce the viscosity of mucines in CF patient's lungs, .

1 Mathematical Model

Designing synthetic biological circuits using genetic elements has become a research field for developing novel biochemical sensors. Specifically Bacterial cell based biosensors have been studied for the environmental monitoring, clinical diagnostics and drug discovery. One of the main challenges for this biosensors to meet real-life applications is the low sensibility and deficient detection limits.

The rise of multiple antibotic resistant bacteria and the evident crisis in drug discovery has become one of the main challenges in human history. Traditional screening not only takes longer times, from years to decades, but often fails to discover novel biomolecules. Bacterial biosensors have provided a novel benchmark for the screening of secondary metabolites producers, boosting the discovery of antibiotics and broadening the spectrum of the latter. One of main aspects that should be considered for the development of novel antibiotic biosensors is the sensibility, since they can only work properly below the minimum inhibitory concentration.

Our project consists of a series of engineered multi-layered transcriptional amplifiers that sequentially increases the output expression level of a GFP reporter protein by the presence of an antibiotic belonging to a specific mechanism of action (MOA) in order to enhanced the process of drug discovery and bacterial screening.

Modelling Biological systems has become an area of interest for multidisciplinary areas of science, medicine and engineering. Mathematical models allow to understand and predict the behavior of complex systems using simple concepts. Bacterial bio-sensors can be divided into three modules, the first comprising a sensing module that recognizes the external signal and transduces into a transcriptional output, the computing module that modulates the transduced sensor signal and the output module which executes the physiological output response. In this project, we develop mathematical models for the engineered multi-layered transcriptional amplifiers which acts as a computing module using both exact deterministic differential equations and stochastic simulations to provide a proof of concept for the amplification signal of the antibiotic biosensor.

The structure of the following sections goes as follows: First we derive the mathematical equations for an already characterized heavy metal biosensor consisting of a constitutive promoter expressing a repressor protein inhibiting the later expression of a reporter gene. Then we will consider the effect of adding a mono-layer orthogonal transcriptional amplifier to the signal amplification. After that we will extrapolate this same models to our antibiotic biosensor.

1.1 Heavy Metal biosensor without cascade amplification

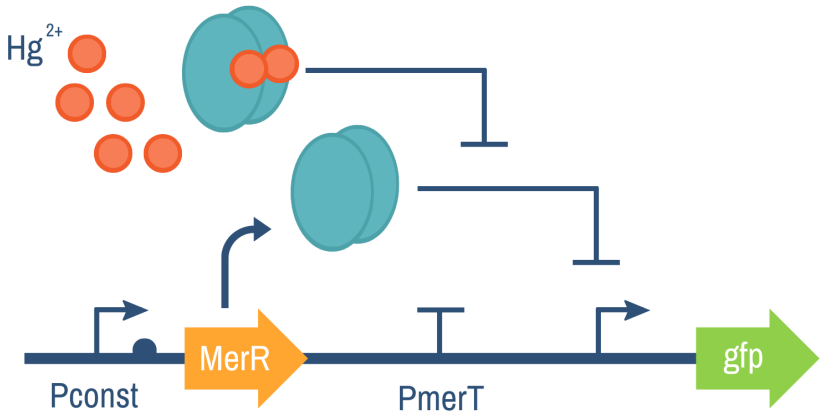

Figure 1: Heavy Metal Biosensor without cascade amplification

The first system to be modeled consist of a two module biosensor (Sensing and Output module) for detecting heavy metals previously characterized. The sensing module is formed by a constitutive promoter that expresses a represor protein. In the absence of heavy metal the repressor protein inactivates the output module consisting on a second promoter upstream to a gfp gene by binding to this regulatory region. Some of the requirements for this system to work correctly is a weak promoter such that in the presence of heavy metal inducer the gfp signal can be turned on efficiently. Another important requirement is that the arsenic-repressor interactions be stronger than the promoter-repressor in order to overcome such inhibition and lower the detection limits of the heavy metal.

The system of differential equations of the system under study is:

$$\frac{dR(t)}{dt} = \alpha_0 + k_{-1}C_1(t) + k_{-2}C_2(t) - R(t)(\delta_R + k_1P(t) + k_2I(t)) \quad (1)$$

$$\frac{dC_1(t)}{dt} = k_1R(t)P(t) - k_{-1}C_1(t) \quad (2)$$

$$\frac{dP(t)}{dt} = -k_1 R(t)P(t) + k_{-1}C_1(t) \tag{3}$$

$$\frac{dI(t)}{dt} = k_{-2}C_2(t) - I(t)(k_2 R(t) + \delta_I) \tag{4}$$

$$\frac{dC_2(t)}{dt} = k_2 I(t)R(t) - k_{-2}C_2(t) \tag{5}$$

$$\frac{dG_(t)}{dt} = \beta_0 + \beta_1 P(t) - \delta_G G(t) \tag{6}$$

Notice that in a chemical equilibrium in (2), the the rate of Repressor-Promoter formation is equal to the rate of dissociation of the later and moreover $\frac{dP(t)}{dt} = -\frac{dC_1(t)}{dt}$. This processes of binding are know to happen at short life times so that an equilibrium between Repressor-Promoter is established so quickly so that their concentrations don't change over time. Therefore a steady state approximation can be proposed. The chemical equilibrium constant $\frac{k_{-1}}{k_1} = \frac{RP}{C_1} = K_{eq1}$ is obtained directly from the steady state assuming $\frac{dC_1(t)}{dt} = 0$. Therefore in chemical equilibrium the terms for promoter occupancy vanish and the differential equation simplifies to:

$$\frac{dR(t)}{dt} = \alpha_0 + k_{-2}C_2(t) - R(t)(\delta_R + k_2 I(t)) \tag{7}$$

$$\frac{dI(t)}{dt} = k_{-2}C_2(t) - I(t)(k_2 R(t) + \delta_I) \tag{8}$$

$$\frac{dC_2(t)}{dt} = k_2 I(t)R(t) - k_{-1}C_2(t) \tag{9}$$

$$\frac{dG_2(t)}{dt} = \beta_0 + \beta_1 P(t) - \delta_G G(t) \tag{10}$$

We can repeat the same process for the formation of inhibitor repressor complex, assuming a steady state for the binding of Inducer to the Repressor Protein. Setting $\frac{dC_2(t)}{dt} = 0$. We obtain a chemical equilibrium constant directly from this assumption $\frac{k_{-2}}{k_2} = \frac{IR}{C_2} = K_{eq2}$, Once again some terms are cancelled out and the system of differential equations simplifies to:

$$\frac{dR(t)}{dt} = \alpha_0 - \delta_R R(t) \tag{11}$$

$$\frac{dI(t)}{dt} = -\delta_I I(t) \tag{12}$$

$$\frac{dG_(t)}{dt} = \beta_0 + \beta_1 P(t) - \delta_G G(t) \tag{13}$$

The analytical solutions of R(t) and I(t) are $R(t) = \frac{\alpha}{\delta_R}(1-e^{-\delta_R t})+R_0 e^{-\delta_R t}$ and $I(t) = I_0 e^{-\delta_I t}$.In steady state R becomes the rate of basal expression and degradation dilution and I becomes zero $R^{ss} = \frac{\alpha}{\delta_R}$. Assuming that the rate of basal expression is approximately zero the last equation becomes

$$\frac{dG(t)}{dt} = \beta_1 P(t) - \delta_G G(t) \tag{14}$$

Knowing $\frac{k_{-1}C_1}{k_1 R} = P$ and $\frac{k_{-2}C_2}{k_2 I} = R$ therefore $P \propto I$ up to an arbitrary constant $P(t) = KI(t)$

$$\frac{dG(t)}{dt} = \beta_1 K I(t) - \delta_G G(t) = \beta_1 K I_0 e^{-\delta_I t} - \delta_G G(t) \tag{15}$$

Using the Laplace Transform $\mathscr{L}\{\frac{dG_(t)}{dt}\} = \mathscr{L}\{\beta_1 K I_0 e^{-\delta_I t} - \delta_G G(t)\}$ and assuming the GFP is initially zero we obtain .

$$G(s)(s+\delta_G) = \beta_1 K I_0 \frac{1}{s+\delta_I} \tag{16}$$

$$G(s) = \beta_1 K I_0 \frac{1}{(s+\delta_I)(s+\delta_G)} \tag{17}$$

Using partial fractions we obtain

$$G(s) = \beta_1 K I_0 \frac{1}{(s+\delta_I)(s+\delta_G)} \tag{18}$$

$$G(s) = \frac{\beta_1 K I_0}{\delta_G - \delta_I}\left(\frac{1}{s+\delta_I} - \frac{1}{s+\delta_G}\right) \tag{19}$$

$$G(t) = \frac{\beta_1 K I_0}{\delta_G - \delta_I}(e^{-\delta_I t} - e^{-\delta_G t}) \tag{20}$$

1.2 Heavy Metal biosensor without cascade amplification

However, this approximations do not satisfy the induction properly, since the expression depends linearly to the initial concentration of inductor, Even though, this model allow us to understand the kinetic behavior of the system. For a better explanation of the induction a simple empirical equation can be obtained by setting the promoter vacancy as $O(R) = \frac{P(t)}{P(t)+C_1(t)} = \frac{K_{eq1}}{R(t)+K_{eq1}}$.

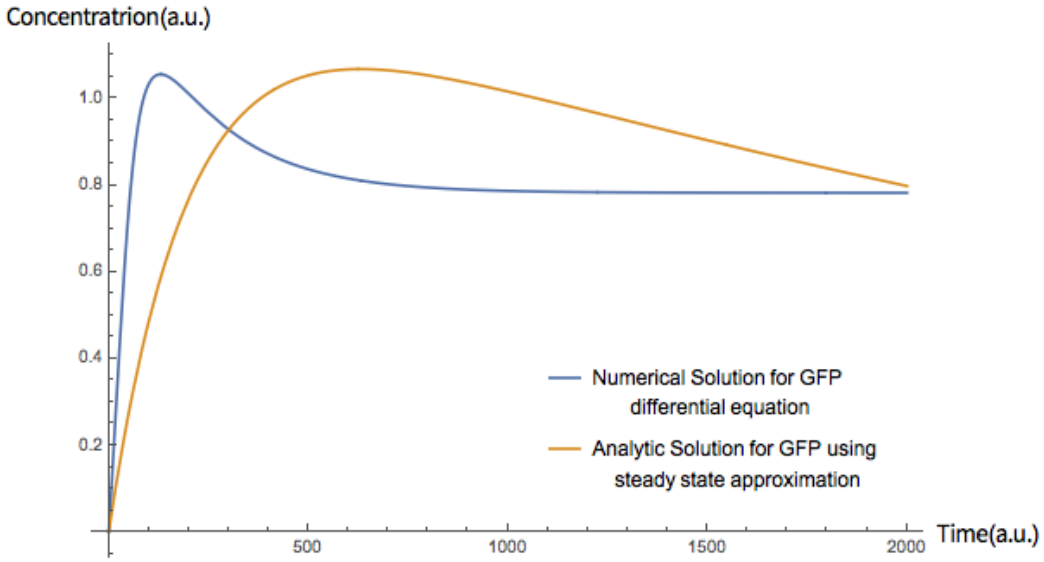

Figure 2: Comparison between Numerical Solution and Analytical Solution

However we are interested on the effect of the inducer on the expression of GFP therefore we can change the promoter de-repression(induction) as $O(I) = \frac{I(t)}{I(t)+K}$ For experimental purposes I(t) can be considered constant at all time, that is, the degradation rate of I(t) is small so that $\frac{dI(t)}{dt} = 0$ and $\delta_I = 0$. The expression of can be adjusted to a Hill-Langmuir function of induction by inserting a parameter n known as the Hill parameter which allows the tuning and sensibility of induction curves.$\frac{I^n}{I^n+K^n}$. The differential equation for the expression of Gfp is:

$$\frac{dG(t)}{dt} = \beta_0 + \beta_1 \frac{I^n}{I^n + K^n} - \delta_G G(t) \tag{21}$$

$$G^{ss} = \frac{\beta_T}{\delta_G} \frac{I^n}{I^n + K^n} \tag{22}$$

1.3 Heavy Metal biosensor with a multilayer- orthogonal transcriptional amplifier

Multi-layer orthogonal transcriptional amplifier have proved to amplified considerably the signal output lowering the detection limits for sensing applications. The system of differential equations for a monolayer- orthogonal transcriptional amplifier consisting of a dimer activator previously studied

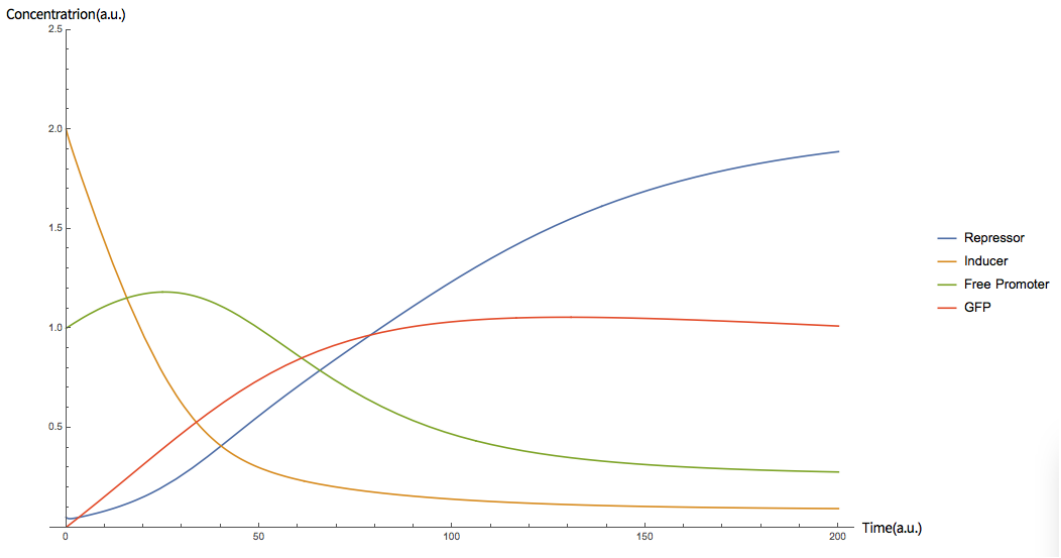

Figure 3: Numerical Solution of system of differential equations without cascade amplification

integrates the following terms.

$$\frac{dH_R(t)}{dt} = \beta_0 + \beta_1 P_A(t) + k_{-3} H_2(t) - H_R(t)(\delta_{H_R} + k_3 H_S(t)) \tag{23}$$

$$\frac{dH_S(t)}{dt} = \beta_0 + \beta_1 P_A(t) + k_{-3} H_2(t) - H_S(t)(\delta_{H_S} + k_3 H_R(t)) \tag{24}$$

$$\frac{dH_2(t)}{dt} = k_3 H_R(t) H_S(t) - k_{-3} H_2(t) \tag{25}$$

$$\frac{dP_B(t)}{dt} = -k_4 H_2(t) P_B(t) + k_{-4} C_3(t) \tag{26}$$

$$\frac{dC_3(t)}{dt} = k_4 H_2(t) P_B(t) - k_{-4} C_3(t) \tag{27}$$

$$\frac{dG(t)}{dt} = \gamma_0 + \gamma_1 P_B(t) - \delta_G G(t) \tag{28}$$

For a bi-layer biosensor the mathematical approach for establishing the differential equations is the same

$$\frac{dH_R(t)}{dt} = \beta_0 + \beta_1 P_A(t) + k_{-3} H_2(t) - H_R(t)(\delta_{H_R} + k_3 H_S(t)) \tag{29}$$

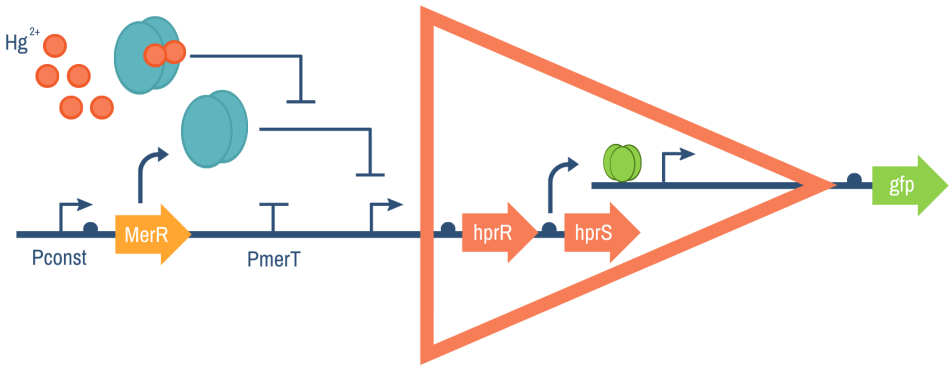

Figure 4: Monolayer orthogonal Amplifier

$$\frac{dH_S(t)}{dt} = \beta_0 + \beta_1 P_A(t) + k_{-3}H_2(t) - H_S(t)(\delta_{H_S} + k_3 H_R(t)) \tag{30}$$

$$\frac{dH_2(t)}{dt} = k_3 H_R(t) H_S(t) - k_{-3}H_2(t) \tag{31}$$

$$\frac{dP_B(t)}{dt} = -k_4 H_2(t) P_B(t) + k_{-4} C_3(t) \tag{32}$$

$$\frac{dC_3(t)}{dt} = k_4 H_2(t) P_B(t) - k_{-4} C_3(t) \tag{33}$$

$$\frac{dE(t)}{dt} = \gamma_1 P_B(t) - \delta_G E(t) - k_5 E(t) P_c(t) + k_{-5} C_4(t) \tag{34}$$

$$\frac{dC_4(t)}{dt} = k_5 E(t) P_C(t) - k_{-5} C_4(t) \tag{35}$$

$$\frac{dP_C(t)}{dt} = -k_5 E(t) P_C(t) + k_{-5} C_4(t) \tag{36}$$

$$\frac{dG(t)}{dt} = \varepsilon_1 P_B(t) - \delta_G G(t) \tag{37}$$

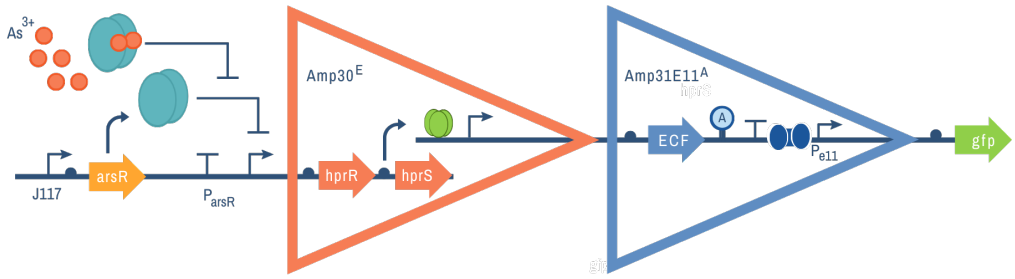

Figure 5: Bilayer orthogonal Amplifier

Instead on trying to find the analytical solutions of the systems of differential equations. We are now interested in comparing the biosensor with and without a multilayer- orthogonal transcriptional amplifier under same circumstances.

Using numerical methods, we solve the system of differential equations applying the same parameters in order to demonstrate as a proof of concept the signal amplification when a multilayer orthogonal transcription amplifier is implicated on the modulation of signal. Even though we do not implicitly determined the sigmoidal behaviour in the differential equations, nevertheless we still observe this behaviour for the bilayer and trilayer amplifier. This is an intrinsic behaviour of the system. As it is shown a gain in signal is obtained when the number of layers is increased however a Horizontal scaling towards higher concentrations are observed. Therefore some other aspects should be considered in the design of a genetic switches. These aspects are characterized in the Hill equation and are further discussed on the section: Response curve-based tuning process for antibiotic biosensor.

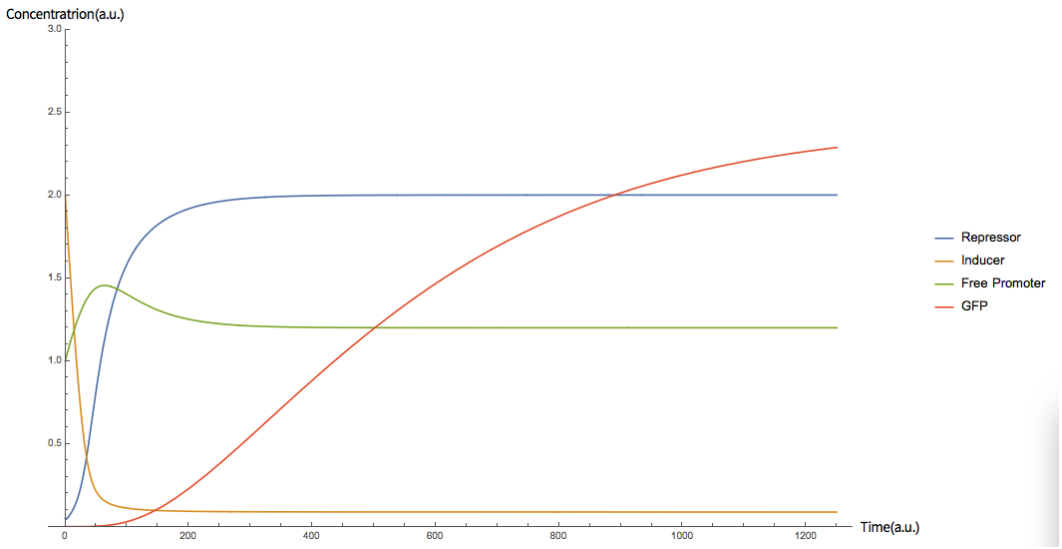

Figure 6: monolayer orthogonal Amplifier Numerical Solution of system of differential equations

1.4 Response curve-based tuning process for antibiotic biosensor

During the last decade, efforts have been made in order to comprehend responses of cellular systems in order to tune the rate of response of such systems. That is, given an input, been able to control the rate of change of an output. Some of the main aspects under study are: How can the shape of the response curve can be altered? How can we mathematically describe such ligand specific behaviour? In the following section we review some mathematical aspects of a semi-empirical formula know as Hill-Langmuir Function. This equation has proof to adjust to numerous biological systems where an input-output response is involved. Therefore understanding the parameters of this equation and how experimentally it is possible to modify them is vital for our project in order to design a genetic circuit capable of detecting low concentrations of antibiotics

The Hill Equation

The Hill Equation is an experimentally equation that refers to occupancy of macro-molecules. It expresses the fraction of molecules bonded as a function of ligand. Depending on the process, that is, if the ligand acts as an inducer (I) or as a repressor (R) the Hill function takes one of the following

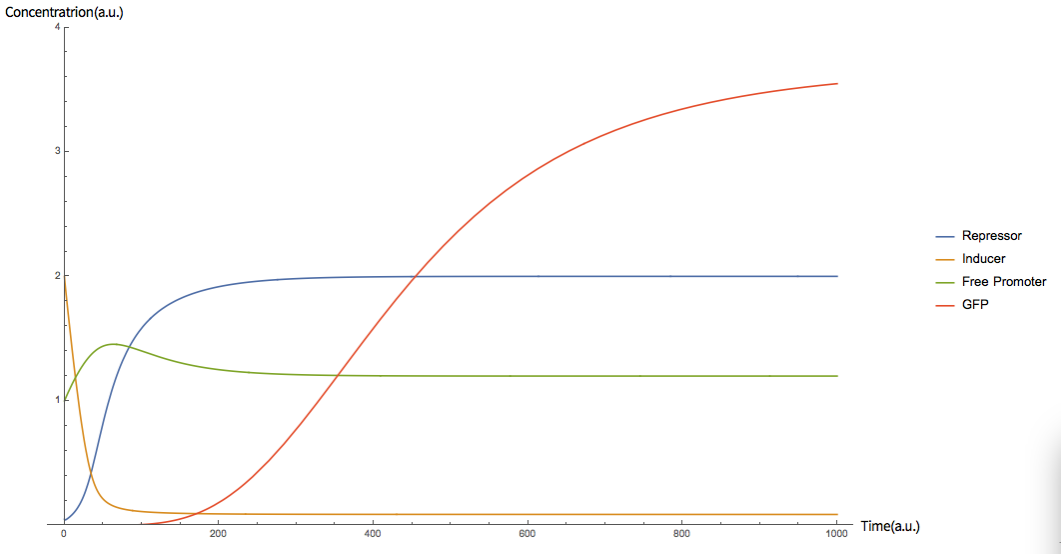

Figure 7: Bilayer orthogonal Numerical Solution of system of differential equations

forms:

$$O(I) = \frac{I^n}{I^n + K^n} \tag{38}$$

$$O(R) = \frac{K}{R^n + K^n} \tag{39}$$

The rate of change of a generic promoter specific ligand transcription under induction is therefore

$$\frac{df}{dt} = \alpha_0 + \alpha_1 \frac{I^n}{I^n + K^n} \tag{40}$$

The parameters K and n, not only are able to adjust the fitting to a broad of experimental data but also have a significant biological meaning. The parameter K is the Hill constant and is related to the dissociation between the ligand and the biomolecule, it is equal to to the ligand concentration where half of the binding sites are occupied. On the other hand the parameter n is known as the Hill parameter. It is related to the cooperative binding, that is the binding affinities when two or more ligands bind to the biomolecule of interest and how this process is enhanced or reduced. An important result of cooperative binding is steepness and sensibility. The higher the n the steeper the response curve and the more sensible to input changes the system

- copia.png

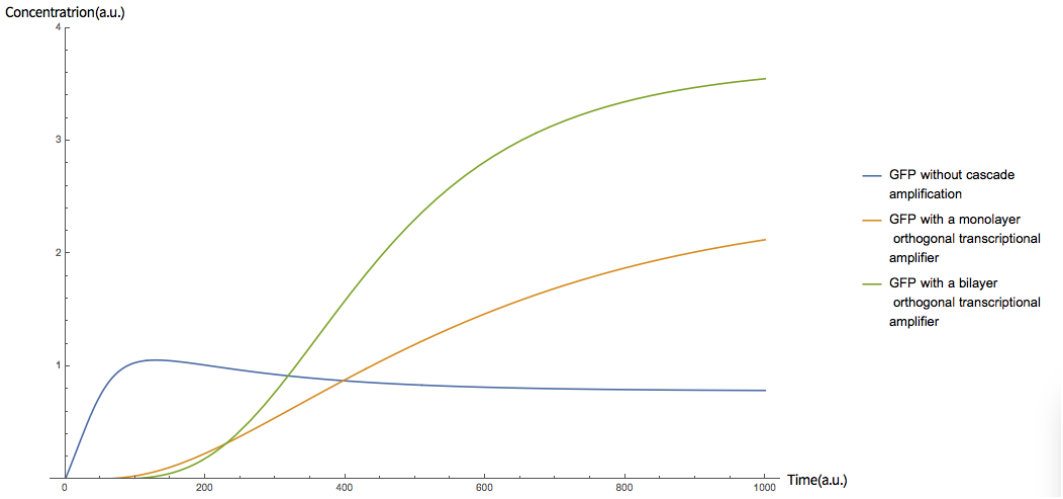

Figure 8: Cascade Amplification

becomes. For induction response systems β_0 is the basal expression and β_1 is the maximum additional production rate under induction effects.

Therefore designing a biosensor with such cooperative in order to be able to detect small concentrations of antibiotics due to minimal inhibitory concentrations and being able to generate an output signal as fast as possible is an important task for our project. On the next sections we will discuss some ways to transform the sigmoidal response curves and how this knowledge guided the construction of the multilayer- orthogonal transcriptional amplifier.

Steepness:

Tuning the Hill coefficient n has a direct effect on the steepness of the response curve. In the limit where n tends to infinite the curve becomes a step function. Therefore having a switch like steady state response curve is synonym of a ultra sensitive process. For transcription of a reporter gene this is related to the participation of multiple transcription factors therefore the first layer of the transcriptional amplifier included the combination of HrpR and HrpS, are two proteins structurally related to the enhancer- binding proteins and acts as a two component regulatory system. Therefore using this system we increase the sensibility of our biosensor.

Vertical Shifting:

Vertical shifting is generated when a constitutive output is found on the system. The constitutive expression of a promoter is directly expressed on β_0 which has units of Concentration s^{-1}. For designing a biosensor that only

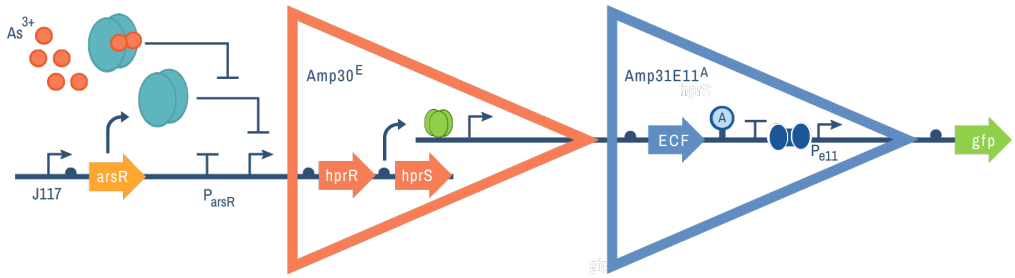

Figure 9: Bilayer orthogonal Amplifier

expresses a signal output under the presence of antibiotics with a specific mechanism of action and be strongly repressed otherwise it is important to choose such promoters that have β_0 almost zero. For the specificity of the needed promoters, we chose to work with ypuA, fabHB, yorB and helD.

Horizontal scaling Horizontal Scaling is directly related to modifying the Hill constant K . As mentioned above, this constant is related to the efficiency of binding of the ligand. Since the Hill constant is equal to the concentration of the ligand where half of the binding sites are occupied the smaller this constant the lower the amount of ligand necessary to turn on the output signal. For improving the detection limits of biosensors it is an important aspects to design systems which reduce as much as possible this constants. For our project lowering as much as possible the effective ligand concentration in order to detect an output signal is necessary since there is an intrinsically disadvantage of using bacteria biosensors because the inhibition of growth above the MIC. Xinyi Wan et al. reported values of K for a double layer biosensor (RS-E11) of 0.065 (uM) and for a double layer biosensor (RS-Rin A) of 0.052 uM approximately, therefore both systems have the parameter K to detect up to 10 nM of Heavy Metals which provides a useful platform for working with antibiotics.

Leakage:

Referring to an up-regulated process(induction) leakage denotes the frac-

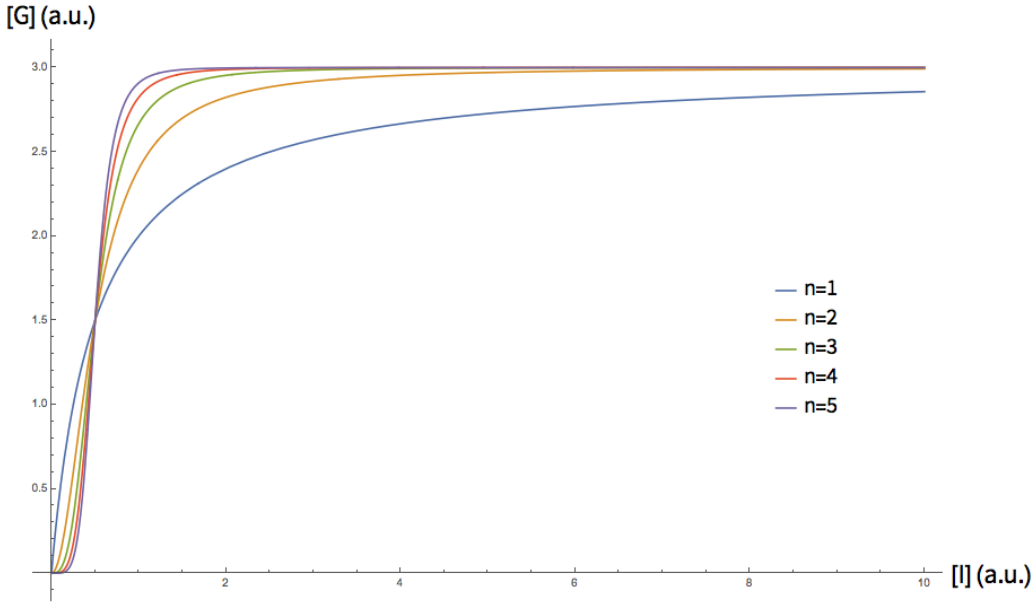

Figure 10: Steepeness

tion of signal that is always activated and cannot be repressed under any circumstance. Therefore under the absence of input there will be a remaining output. This phenomena is characterized by vertical shifting without affecting the maximal output. Mathematically this is represented by the simple relation $\beta_0 + beta_1 = constant$. Experimentally tuning this effect is not well understood but it involved both the presence of a basal transcription and a induction transcription.

Vertical extension :

Vertical extension or amplified signal output is characterized by an increase in the output signal maintaining fixed the low end level. The parameter beta1 can be seen as a signal amplitude over time. Increasing b1 significantly increases the output signal. For up-regulated systems this can be achieved by increasing the probabilities of binding by transcription factors that bind the RNA polymerases.

In this case some fundamental factors that increase the output signal of the amplification cascade would be the presence of proteins such as hrpR and hrpS, with a transcriptional binding function. Sigma factors are proteical subunits of bacterial RNA polymerases that allow the specific determination of promoter DNA binding and an efficient transcription. Therefore the use of a Sigma factor in the second layer of the cascade provides a β_1 of 61119

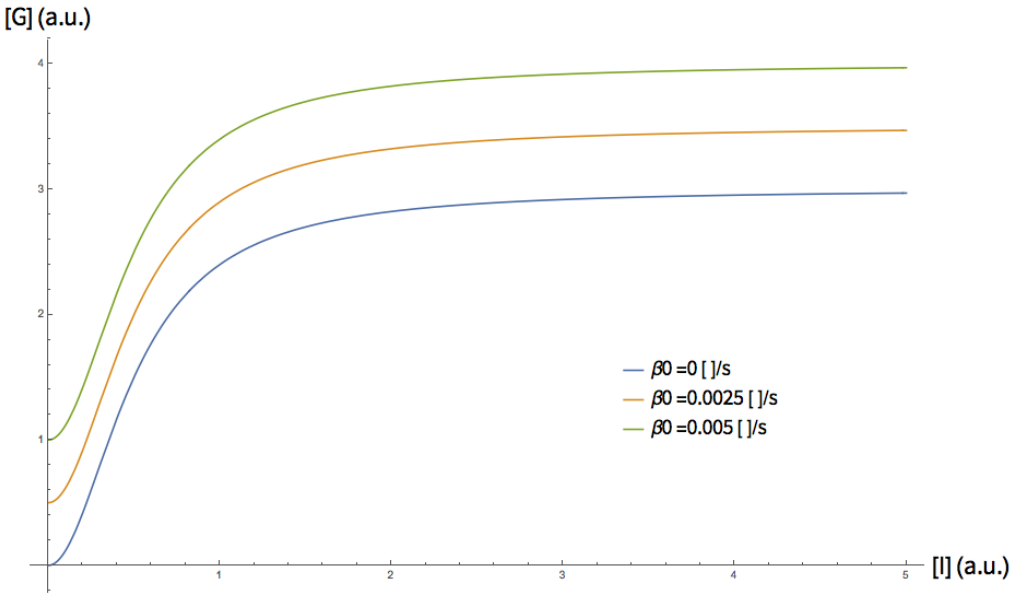

Figure 11: Vertical shifting

(a.u.) in contrast the (RS-RinA) bilayer amplifier that has a β_1 of 59252 (a.u). Therefor the use of a (RS-S11) assures us a better amplification of the signal.

Mathematical equations are powerful tools for explaining biological phenomena. Simple mathematical descriptions such as the Hill Langmuir equation, characterizes by simple parameters should be considered on the design of genetic circuits with sensing applications. Mathematical knowledge and biological implications of simple parameters allow us to improve the design of a multilayer-orthogonal transcription amplifier, allowing us to select biological parts that increase the steepness of our signal output reduce the vertical shifting and leakage, increase the horizontal scaling and vertical extension of our response curves. Finally, we would like to mention the huge impact our mathematical modelling had on the design of our genetic circuit, because it provided us the knowledge in order to decide which elements include in our transcriptional amplifier cascade, changing our vision and defining important elements of the wet lab work.

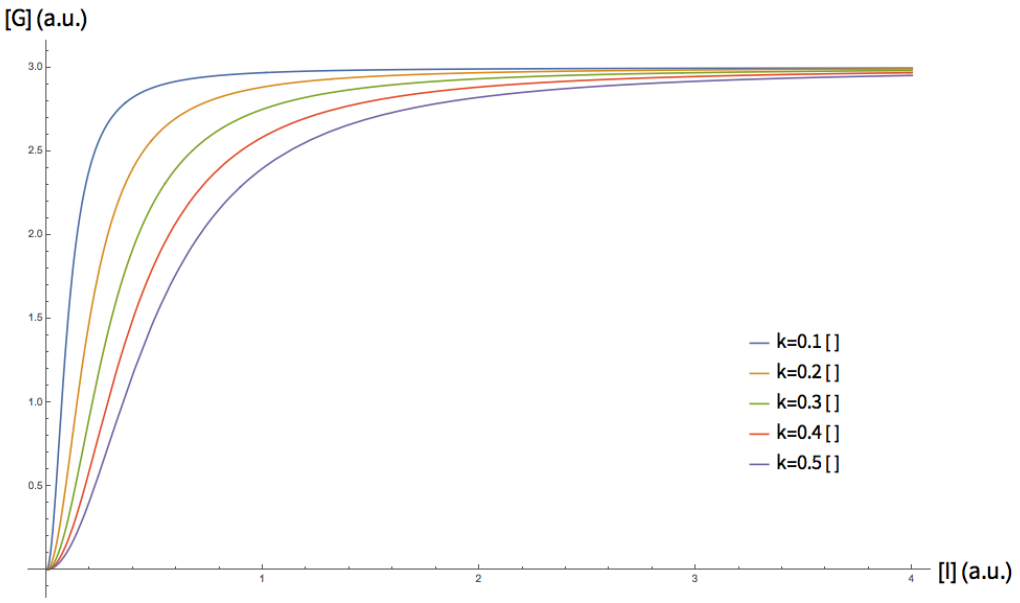

Figure 12: Horizontal scaling

1.5 Inducible expression in E. coli T7 System for the production of Sialidase mucolytic

Cystic fibrosis(CF) is a progressive genetic disease that, through the production of abnormally thick mucus, causes degeneration of lung conditions and induces the proliferation of multidrug resistant bacterial strains (MRBS). Mucolytic agents have proved to increase the effectiveness of cough, therefore, a treatment combining antibiotics with mucolytics is a promising strategy for improving the health conditions in CF patients. The main components of the mucus are the mucins; proteins which present a high amount of sialic acid due to the frequent infections patients are exposed to, Therefore we choose an enzyme capable of breaking such residues; the neuraminidase from Micromonospora viridifaciens . We decided to implement a super-folding green fluorescent protein (sfGFP) because of its secretory activity. This constructs are under the control of a T7-LacO promoter and C-terminal 6His-tag, which will facilitate the recovery of the sialidase from the medium. In this section, we develop a mathematical model for the T7-LacO promoter and the secretory activity of the SfGfp.

In a T7 express strain, a lacI gene constitutively expresses a repressor protein which represses the lac Operon. Moreover, a RNA polymerase gene is inserted into the lac Operon on the E. coli chromosome and is expressed under

- copia.png

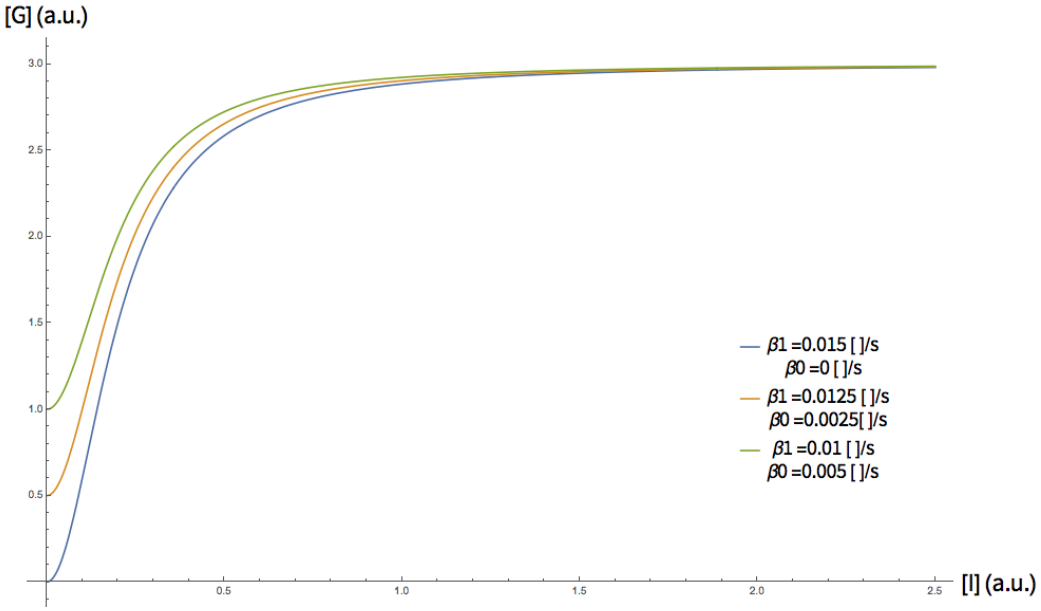

Figure 13: Leakage

the control of the lac promoter. Therefore, under the absence of IPTG, there is a strong repression of T7 RNA polymerase and only leaked expression is maintained. The lac Operon consist of three genes, the gene lacZ that codes for a β galactosidase ,the gene lacY that codes β galactosidese permease and the gene lacA that codes for a β galactoside transacetylase. Unlike lactose, IPTG cant be metabolized into allolactose but directly binds the lac repressor. Thus IPTG induces the expression of lac operon. Additionally, a positive feedback is generated by β galactosidese permease which transport the external IPTG to the citosol. Another consideration for the mathematical model is that lac repressor is able to repress the expression of genes regulated by the T7 promoter on the plasmid. Considering a chemical equilibrium between the binding of the repressor to the promoters $\mathrm{R} + \mathrm{P} \rightleftharpoons \mathrm{RP}$ we have that the fraction unrepressed is $O(R) = \frac{P(t)}{P(t)+RP(t)} = \frac{K}{R(t)+K}$. The transcription lacY and T7 is:

$$\frac{dY}{dt} = \alpha_0 + \alpha_1 \frac{K_1}{R(t) + K_1} - \delta_Y Y(t) \tag{41}$$

$$\frac{dT}{dt} = \alpha_0 + \alpha_1 \frac{K_1}{R(t) + K_1} - \delta_T T(t) \tag{42}$$

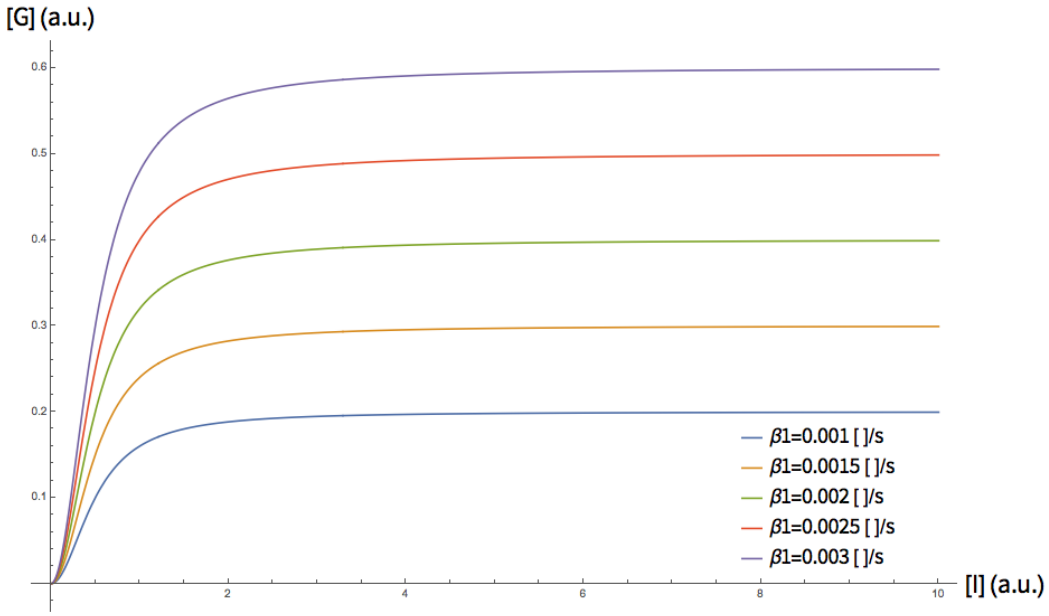

Figure 14: Vertical extension

The total concentration of IPTG is $IPTG_0 = IPTG_e(t) + IPTG_i(t)$ and remains constant at all time. Therfore the external concentration of IPTG is $IPTG_0 - IPTG_i(t) = IPTG_e(t)$ Assuming a Michaelis Menten kinetics for the uptake of IPTG then the differential equation is:

$$\frac{dI_{int}}{dt} = \frac{k_I Y(t)(I_0 - I_{int}(t))}{K_M(t) + I_0 - I_{int}(t)} - \delta I_{int}(t) \tag{43}$$

$$\frac{dR}{dt} = \beta_0 + \beta_1 \frac{K_2}{K_2 + I_{int}(t)} - \delta_R R(t) \tag{44}$$

In steady state the concentration of R is:

$$R^{ss} = \frac{\beta_{Tot}}{\delta_R} \frac{K_2}{K_2 + I_{int}(t)} \tag{45}$$

The expression of superfolder GFP on the plasmid with the regulation of the T7 promoter is

$$\frac{dS_i}{dt} = \gamma_0 + \gamma_1 \frac{T(t)}{K_3 + T(t)} - \delta_S S(t) - k_S S_i(t) \tag{46}$$

$$S_i^{ss} = \frac{\gamma_{Tot}}{\delta_S + k_S} \frac{T(t)}{K_3 + T(t)} \tag{47}$$

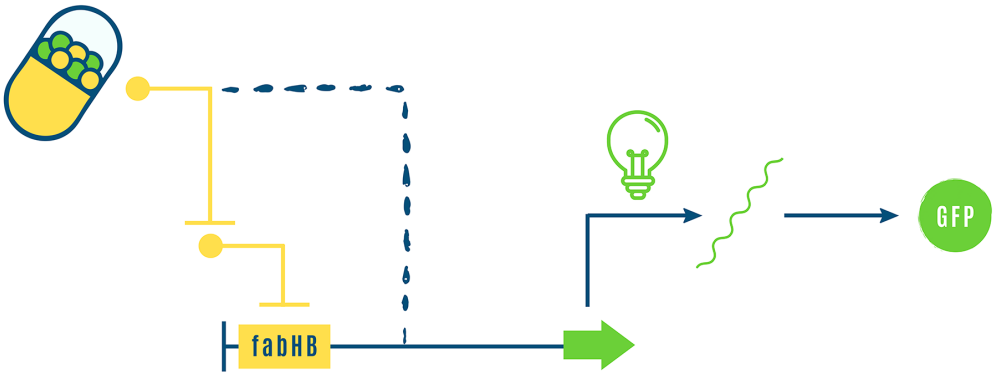

Figure 15: Antibiotic-Response Promoter fabHB regulates the expression of gfp reporter gene. In the presence of an antibiotic with an specific mechanism of action(i.e. DNA synthesis, RNA synthesis, Protein synthesis, etc.) the expression of gfp will turned on

de GFP(4).png

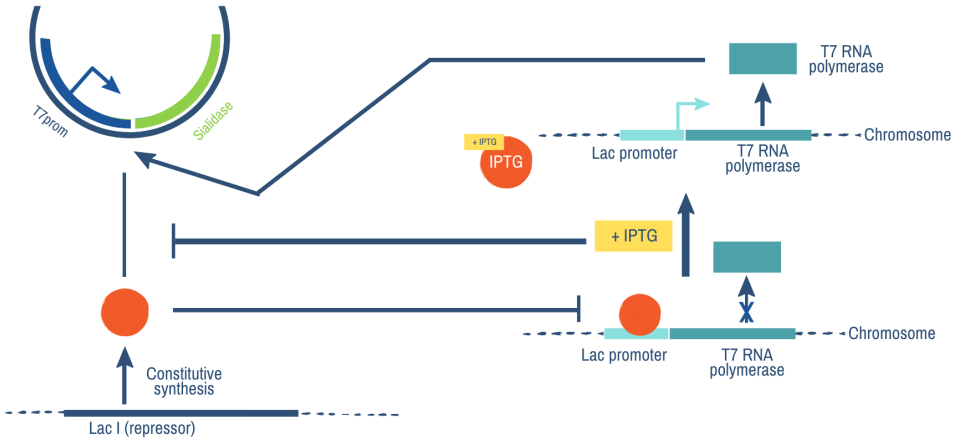

Figure 16: T7- LacO system induction by IPTG

The rate of secretion of the SfGFP is

$$\frac{dS_e}{dt} = k_S S_i(t) - \delta_S S_e(t) \tag{48}$$

in steady state the amount of SfGFP is:

$$S_e = \frac{k_S S_i^{ss}}{\delta_S} = \frac{k_S}{\delta_S} \frac{\gamma_{Tot}}{\delta_S + k_S} \frac{T(t)}{K_3 + T(t)} = K_{obs} \frac{T(t)}{K_3 + T(t)} \tag{49}$$

In steady state

$$T^{ss} = \frac{\alpha_{Tot}}{\delta_T} \frac{K_1}{R(t) + K_1} \tag{50}$$

Making a substitution in R in terms of I it can be shown that T is linearly proportional the concentration of SfGFP secreted. Experimentally we can make a curve fitting knowing that the presence of IPTG indirectly induces the expression of T7 RNA polymerase using the following expression :

1.6 Fitting Parameters

Experimentally we validated our induction system using equation

$$S_e^{ss} = k' + k'' \frac{I}{K + I} \tag{51}$$

First we make a kinetic study of the induction of IPTG (0, 40, 200 and 400 uM) upon our constructs of SfGfp and SfGfp-Sialidase measuring the fluorescence in a microplate reader at wavelengths of 485 nm for excitation and 528 nm for emission. This measurements were made by triplicate under 0 hrs , 1 hr, 1 hr . 30 min, 2hrs, 2 hrs 30 min and 3 hrs. The averages were calculated and plotted against time

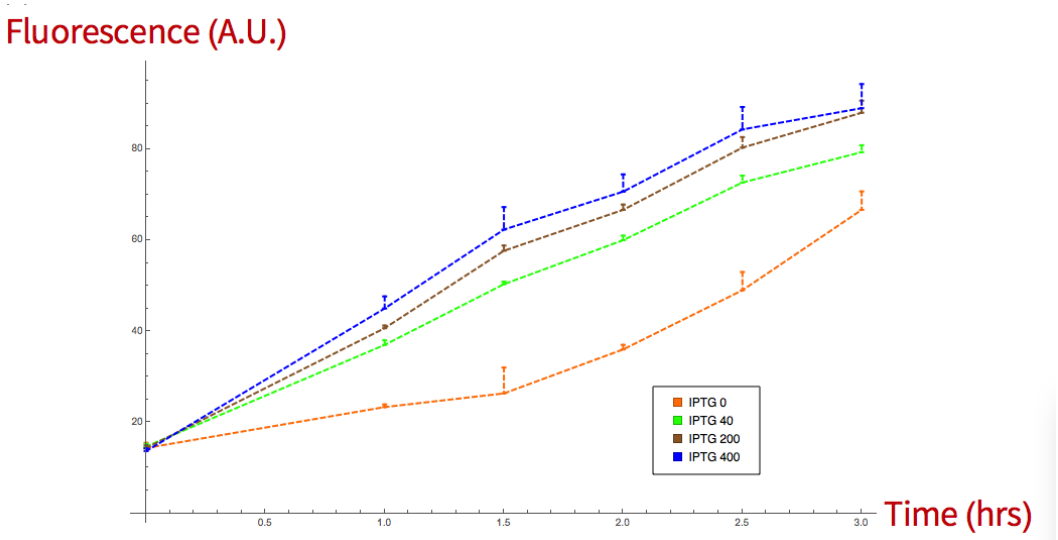

Figure 17: Fluorescence of SfGFP

Then the effect of the induction was plotted against GFP fluorescence at different hours.

We make a nonlinear model fit using Mathematica software from Wolfram Alpha adjusting the experimental data to the equation 51.

The following expression was obtained at 2.5 hours for the fluorescence of SfGFP-Sialidase

$$F_{sfgf-psial} = 4.5008 + 2.96375 \frac{I}{11.3259 + I} \tag{52}$$

For the expression of SfGfp at 2.5 hours we have

$$F_{sfgfp} = 32.1928 + 25.2714 \frac{I}{18.5078 + I} \tag{53}$$

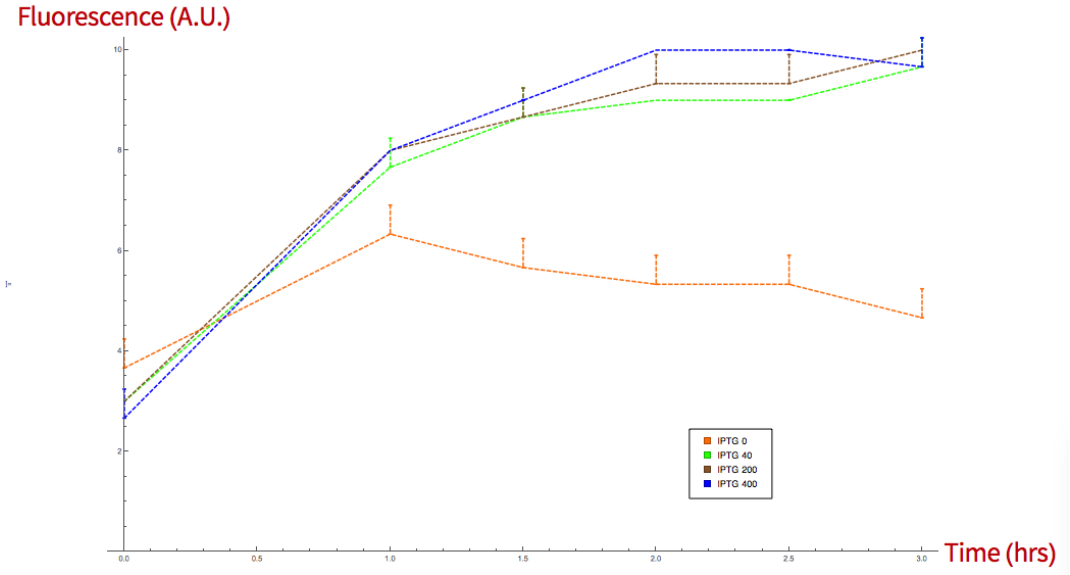

Figure 18: Fluorescence of SfGFP-Sialidase

Even though the Lac repressor strongly represses both THE T7 promoter and the Lac Operon we can see how a basal expression mathematically represented on k_0 is present. However while in the SfGfp-sialidase fusion protein this term keeps almost constant having an estimate value around 4, for the sfGfp alone the first constant increases over time. We hypothesize that this is because of a significant decrease of the secretory activity of the SfGfp is fusioned with other proteins. Further experimentation is needed in order to confirm this hypothesis.

1. Tuning Response Curves for Synthetic Biology. Jordan Ang, Edouard Harris, Brendan J. Hussey, Richard Kil, and David R. McMillen ACS Synthetic Biology 2013 2 (10), 547-567 DOI: 10.1021/sb4000564

2. Urban, A., Eckermann, S., Fast, B., Metzger, S., Gehling, M., Ziegelbauer, K., â Freiberg, C. (2007). Novel whole-cell antibiotic biosensors for compound discovery. Applied and environmental microbiology, 73(20), 6436â6443. doi:10.1128/AEM.00586-07 1.1

3. Wan, X., Volpetti, F., Petrova, E., French, C., Maerkl, S. J., Wang, B. (2019). Cascaded amplifying circuits enable ultrasensitive cellular sensors for toxic metals. Nature Chemical Biology, 15(5), 540â548. doi: 10.1038/s41589-019-0244-3

4.Ingalls, B. P. (2013). Mathematical modeling in systems biology: an introduction. Cambridge, Massachusetts: MIT Press.

5. Santillán, M., Mackey, M. C., Zeron, E. S. (2007). Origin of bistability in the lac Operon. Biophysical journal, 92(11), 3830â3842. doi:10.1529/biophysj.106.101717

6.Alon, U. (2007). An introduction to systems biology: design principles of biological circuits. Boca Raton, FL: Chapman Hall/CRC

1.7 Microfluidics Model

Introduction Compared to single phase flows, microfluidic two-phase flows relies on several physical phenomena that need to be controlled for the droplets to fully form. The flow properties in microchannels rely on three parameters: the channel geometry, the properties of both fluids, and the flow conditions. These factors can be described by some important dimensionless parameters.

Dimensionless numbers The physics behind microfluidics include the relations between the interfacial tension, inertial forces and the involved fluidsâ properties. Dimensionless numbers have become a standard manner to compare fluid interaction at macro and micro scale.

The flow in microfluidic systems are usually characterized by low Reynolds number values, which describes the ratio between inertial and viscous forces in fluids, and can be used to characterize the system.

$$Re = \frac{\rho V L}{\mu} \tag{54}$$

Where ρ is the density of the fluid (kg/m3), V is the average fluid velocity (m/s), L is the linear dimension (m) and μ is the dynamic viscosity of the fluid (kg/ms). In microfluidic systems, viscous forces (μ) dominate and Reynolds numbers are generally smaller than 100, leading to the prevalence of laminar flow. For Re « 1 the flow is dominated by viscous stresses and pressure gradients, hence inertial effects are negligible, and the trajectories of fluidic particles can be controlled precisely.

The dominant forces at the microscale are interfacial and viscous forces, therefore it is important to determine the relative importance of the interfacial tension compared to other forces in droplet generation. The capillary number Ca is the ratio of viscous stress to capillary pressure:

1.2

$$Ca = \frac{\eta \mu}{Y} \tag{55}$$

Here η is the viscosity of the fluid in the two-phase system, μ is the velocity of the phase, and Y is the interfacial tension of the liquid-liquid interface. At low Ca (<1) the interfacial tension dominates, and spherical droplets are found. In contrast, at high Ca (»1) the viscous forces play an important

role, leading to deformation of the droplets and sometimes to asymmetric shapes. Suryo Basaran had previously reported a phases map in which different droplet generation regimes were identified at different ranges of Ca numbers for both continuous and disperse phases. The squeezing regime generates well-rounded monodisperse droplets at high throughput and has defined boundary conditions for the Ca numbers as shown in the figura. Hence a prediction can be made based on the parameters considered in the Ca in order to generate monodisperse droplets in the squeezing regime.

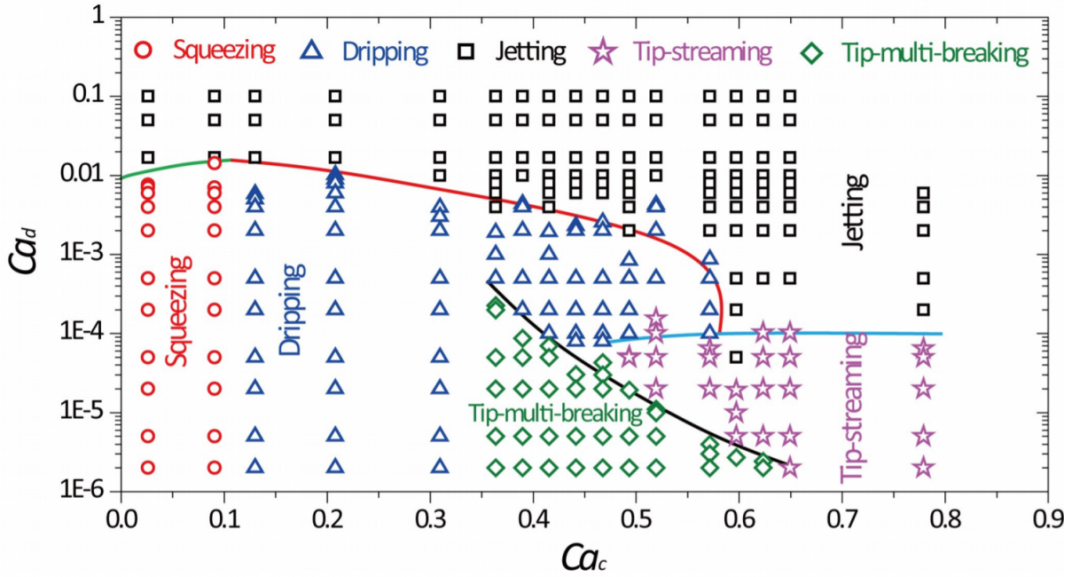

Figure 19: Phase diagram in (Cac,Cad) plane for various modes observed in microcapillary devices.

Interfacial effects The interfacial effects become relevant when working at microscale and are crucial in multi-phase flows. The interfaces considered in microfluidic two-phase systems include the fluid-wall and fluid-fluid interfaces. The wetting properties of the fluid-wall interface are important to determine whether there will be an ordered droplet production or not. If there is a complete wetting of the continuous phase in the microchannels, an orderly pattern can be achieved. The hydrophobicity or hydrophilicity of a solid surface can be expressed quantitatively by contact angles. The contact angle between a liquid and a solid is the angle formed by the tangent from the contact point along the gas-liquid interface. If the contact angle between a liquid and a solid is $<90°$ the liquid will wet the surface and spread over it. If the contact angle is $\geq 90°$, the liquid will stay on the surface as a bead.

Therefore, the* contact angle between a liquid and a solid is dependent on the nature of the liquid as well as the surface characteristics of the solid. Water-in-oil (W/O) droplets can be achieved in hydrophobic surfaces that have a contact angle higher than 90°, in which the droplet will not spread over the surface; nevertheless, it is possible to modify the contact angle by adding surfactants at different concentrations.

Surfactant effects

Surfactants are often used in order to modify the contact angle between the fluid-wall interface. They are also used to reduce the interfacial tension between fluids and to prevent the coalescence or merging of droplets [13]. In the presence of surfactants, the interfacial tension is determined by the competition between interfacial deformation and surfactant convection, diffusion and adsorptionâdesorption kinetics during droplet generation [3]. A faster interfacial deformation and slower mass transfer process causes the surface coverage of surfactants to become smaller, thereby the interfacial tension turns larger [13].

Properties of the fluids (i.e., viscosity, density, interfacial tension) and design parameters (i.e., geometry, dimensions, flow rates) are the main variables responsible for the formation of continuous monodisperse droplets in a microfluidic system.

The droplet breakup process in microfluidic devices has been extensively studied, and several mechanisms have been classified based on the droplet generation. The most important mechanism is the squeezing regime, since this produces continuous monodisperse droplets in defined intervals of time.

The droplet breaking process is not fully understood since it is dependent on many parameters, nevertheless a good approximation can be made based on design parameters including flow rate, viscosities, and geometry of the device.

As the viscous forces and capillary forces are the dominant forces in the droplet breakup and capillary numbers relate those terms, they are essential in the determination of design parameters for droplet formation. Based on the known physical parameters of the fluids being used, it can be possible to calculate the best velocities at which the fluids begin the droplet formation in the squeezing regime.

A MATLAB script was developed in order to determine the optimized velocities and hence the flow rates for droplet generation based on the boundary conditions of the squeezing regime. The following figure is an example of the scatter map created based on the conditions available in literature, the physical parameters of the fluids (interfacial tension, density, and kinematic viscosity), and the geometry of the channel (width and length). The flow rate conditions were used as parameters into a COMSOL simulation in

order to determine the optimized flow rates that could generate continuous monodisperse droplets in order to try them in the experimental section of the microfluidic device.

Simulations and model

As previously discussed, the role of viscosity, effect of flow rates, and geometries of the microfluidic device are of great relevance on droplet formation [1]. Nevertheless, the experimental and empirical investigations that focus on these effects are usually subject to spend a large amount of resources, time, and effort in order to achieve an optimized set of conditions for droplet generation, since there is a high chance of failure at initial stages of the design process [2], [3]. Therefore, a numerical study of microdroplet generation could provide a suitable model for the prediction of the effects of the previously mentioned parameters on a droplet generation T-junction microfluidic device.

A reliable simulation may be a suitable method to reduce the required time to achieve an optimized characteristic of the system, and to be able to forecast how the different modifications of the parameters will impact on the droplet generation [3]. In order to determine the effect of different flow rates of both phases and their relation to droplet size and monodispersity, simulations were carried out using COMSOL Multiphysics which includes a computational fluid dynamics (CFD) module and a microfluidics module as well [4]. CFD provides a reliable alternative in order to obtain insights into a complicated process. Several methods have been typically used in order to simulate two-phase fluidic systems, including volume of fluid (VOF) method, level-set method (LS), phase-field method, and lattice-Boltzmann method. Although there are several advantages regarding the different methods, the LS method represents the interface by a smooth function, and it is convenient for calculating the curvature and surface tension forces [5]. Hence, it seems to be suitable for modeling droplet breakup process in microfluidic devices. In the proposed simulations, we employed LS method to study the droplet-breakup process using FC40 as the continuous phase, and water as the dispersed phase. The effects of the capillary number (Ca) and the different flow rates are investigated [3]. COMSOL Multiphysics determines the modules that are needed in order to give solving parameters, the dimensions in which the experiment will be performed, and the definition of the physics of the problem. For this simulation, we used a laminar two-phase flow using the level set method. A single-phase flow system is less complicated to model computationally than the multiphase flow due to fewer partial differential equations that need to be solved parallelly. Nevertheless, it is needed a two-phase system in order to properly simulate the relationship between the dispersed and continuous phases. In order to analyze the motion of a liquid,

the starting equation to use is the Navier-Stokes equation. The following assumptions are made in order to simplify the model: a constant fluid density, a laminar flow regime exists throughout the system, all fluids are Newtonian, and three-dimensional stresses for a fluid obey Hookeâs law [6]. While assuming the above, the incompressible form of the Navier-Stokes equation is as follows:

$$\rho\frac{du}{dt} + \rho(u \cdot \nabla u)u = \nabla \cdot [-pI + \mu(\nabla u + \nabla u^T)] + F_g + F_{st} \tag{56}$$

As previously described, microfluidic flows have a low Reynolds number, in which viscous forces dominate over inertial forces. So, the inertial variables $\rho(u \cdot \nabla)$ be removed from the above equation. At low Reynolds numbers and small length scale, the relationship between the gravitational forces to surface tension are small enough that the gravitational force is negligible. The terms related to inertia and body forces are removed from the original Navier-Stokes equation, giving:

$$\rho\frac{du}{dt} = \nabla \cdot [-pI + \mu(\nabla u + \nabla u^T)] + F_{st} \tag{57}$$

Multiphase flow has the previously mentioned properties, the boundary conditions at the fluid interface, contact angle, surface tension force, interfacial flows, and time dependent. When computational modeling two-phase flow, another set of equations are necessary. The level set method is used for multiphase simulations and is described further on in the next section. The level set method is a simple and straightforward method for modeling multiphase flow. The level set method uses a smooth signed distance function to produce an interface. The level set variable is represented by ϕ. In phase 1, the value of ϕ in the dispersed phase is equivalent to one. At the interface, which is the region that separates both phases, the level set variable is 0.5, while phase 2 is composed of the continuous fluid and ϕ equals 0. The level-set equation is expressed as:

$$\frac{\partial\phi}{\partial t} + u^{\rightarrow} \cdot \nabla\phi = \gamma\nabla \cdot (\epsilon\nabla\phi - \phi(1-\phi)\frac{\nabla\phi}{|\nabla\phi|} \tag{58}$$

In this equation, γ and ϵ are the stabilization parameters: ϵ determines the thickness of the interface where ϕ goes smoothly from 0 to 1, and it should have the same order as the computational mesh size of the elements where interface propagates. The parameter γ determines the amount of reinitialization of the level set function. A suitable value for γ is the maximum value of the velocity field of the velocity. The interfacial variables, the unit

normal to the interface and the curvature κ , then can be calculated by the following equations respectively:

$$\hat{n} = \frac{\nabla\phi}{|\nabla\phi|} \tag{59}$$

$$\kappa = -\nabla \cdot \hat{n}|_{\phi=0.5} \tag{60}$$

The surface tension force acting on the interface between the two fluids is:

$$\vec{F}_{sf} = \sigma\kappa\delta\hat{n} \tag{61}$$

where σ is the interfacial tension coefficient (N/m), κ is the curvature calculated previously. δ is a Dirac delta function concentrated to the interface. The δ function is approximated by a smooth function according to:

$$\delta = 6|\nabla\phi||\phi(1-\phi)| \tag{62}$$

The density ρ and viscosity μ in the Navier-Stokes equation are smoothed by ϕ across the interface by the following:

$$\rho = \rho_1 + (\rho_2 - \rho_1)\phi \tag{63}$$

$$\mu = \mu_1 + (\mu_2 - \mu_1)\phi \tag{64}$$

The finite element analysis (FEA) is a numerical method to solve partial differential equations. The finite element method relies on meshing the spatial domain into multiple elements. A finer mesh has a higher number of elements and can provide a more accurate solution but will require a longer computing time than a coarse mesh [3]. FEA uses an iterative process in order to calculate a solution to all couple field variables. This modeling in order to be used needs a geometry, then models, material properties, and boundary conditions are applied to the geometry, and finally meshed. Then, computation begins, and the algorithms try to converge in order to give a solution. The first design is a three-dimensional T-junction composed of two inlets. The inlet for Fluid 1 had a width of 100 μm and a length of 400 μm prior to the junction. The inlet for Fluid 2 had an inlet width of 100 μm and length of 300 μm prior to reaching the junction, as can be seen in the following figure. Post T-junction, the droplets travel 600 μm to the expanded pillar induced merging chamber. The entire geometry has a depth of 100μm.

A free tetrahedral mesh with a COMSOL Multiphysics® predetermined element size of âfineâ was utilized. Then a mapped operation was performed over the different distribution elements of the geometry in order to have

smaller features in the interface section. Finally, a swept function was used to generate the different regions of the mesh size in the model.

The properties of fluids utilized in the three-dimensional study can be seen below in Table I. The flow rate of the continuous phase is not constant but varies from 1 $\frac{\mu l}{min}$ to 50$\frac{\mu l}{min}$. The variables for the oil are based on the specification for FC40.

The main goal of the simulation is to generate droplets. Droplet generation commonly occurs by shearing one fluid phase with another. Utilizing the T-junction defined previously with the parameters based on the MATLAB script. All physical parameters are based on literature. Since the goal was to see whether the conditions could generate droplets or not, the results are only qualitative with a binary response on whether or not a droplet was formed. The next steps for this simulations were to test the given parameters that could make droplets in the experimental setup.

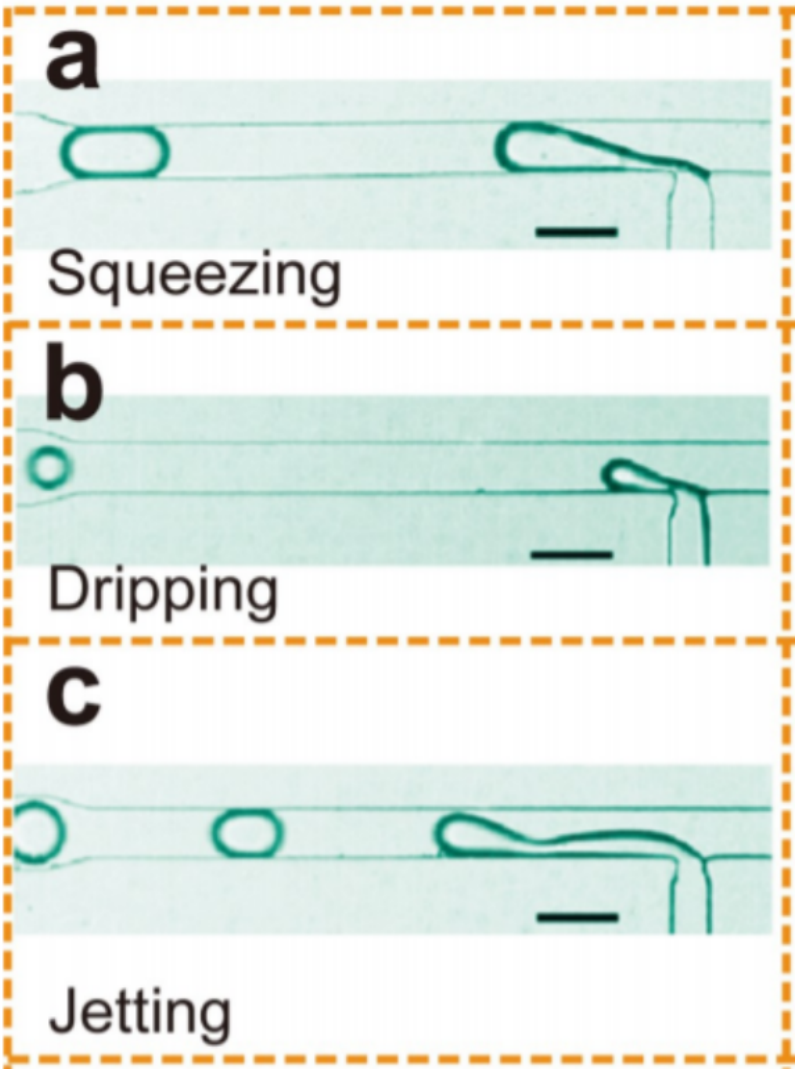

Figure 20: Regimes

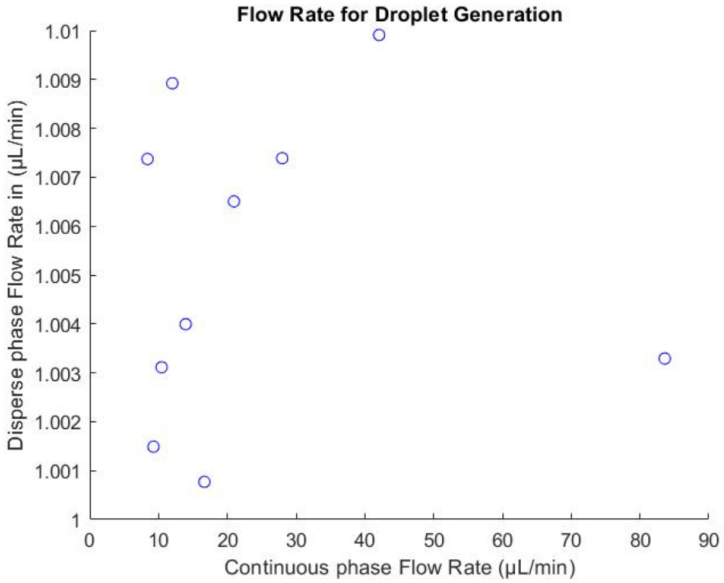

2.png

first design.png

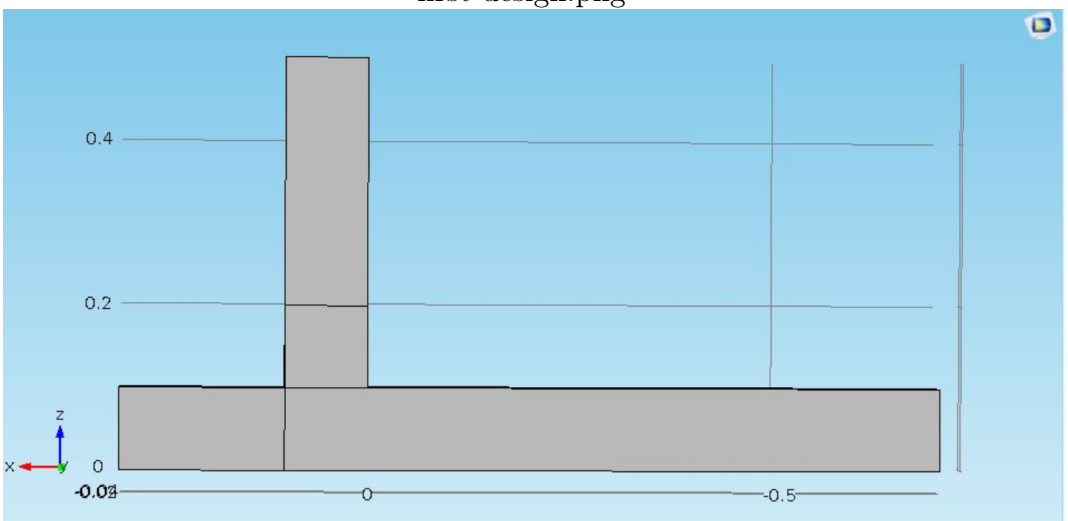

free tetrahedral.png

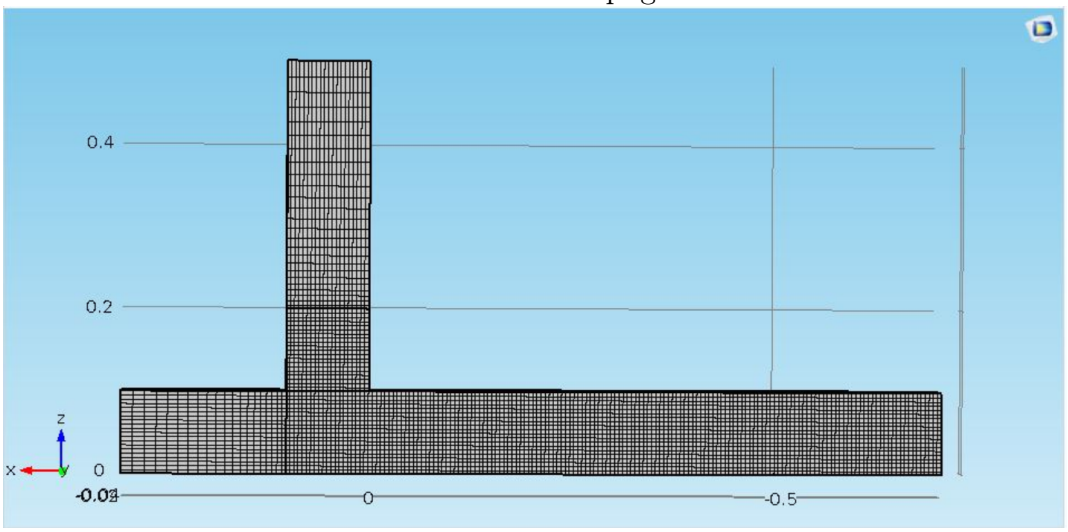

Figure 21: Properties of fluids used in three-dimensional study.

properties of.png

Variable	Numerical Value	Units	Description
Q_c	3.42	µL/min	continuous phase
Q_d	1.16	µL/min	disperse phase
Viscosity oil	$3.4*10^{-3}$	Pa*s	carrier fluid
Density oil	$1.85*10^{3}$	kg/m^3	carrier fluid
Viscosity aqueous	$1*10^{-3}$	Pa*s	droplet
Density aqueous	$1*10^{3}$	kg/m^3	droplet
Π	0.5	a.u.	Level-set parameter
γ	0.05	m/s	Reinitialization parameter
ε	$5*10^{-6}$	m	Interface thickness
Contact angle	100	Degrees	
Interfacial tension	$2.87*10^{3}$	N/m	